Systematic Design Methodology and Construction of Micro Aerial Quadrotor Vehicles

11

Swee King Phang, Kun Li, Ben M. Chen, and Tong H. Lee

Contents

Abstract

This chapter presents a guideline to systematically design and construct an ultralight micro aerial quadrotor vehicle, capable of autonomous flight. The guideline details the steps to design a stable quadrotor with not more than 50 g takeoff weight while having a flight duration of 8 min. Optimization was done to all mechanical parts of the vehicle with the constraints of its weight and

S.K. Phang • K. Li
Control and Simulation Lab, National University of Singapore, Singapore
e-mail: king@nus.edu.sg; kunli89@nus.edu.sg

B.M. Chen • T.H. Lee
Control and Simulation Lab, Department of Electrical and Computer Engineering, National University of Singapore, Singapore
e-mail: bmchen@nus.edu.sg; eleleeth@nus.edu.sg

K.P. Valavanis, G.J. Vachtsevanos (eds.), *Handbook of Unmanned Aerial Vehicles*,
DOI 10.1007/978-90-481-9707-1_116,

its performance. The guideline first covers the structural analysis of the micro quadrotor air frame, followed by its design in a 3D virtual simulator. Then, design of avionic system such as processor and sensors will be discussed, followed by controller implementation with the aid of software simulation. Components of the micro quadrotor are then fabricated and implemented based on the optimum results obtained from various simulations. Finally, the feasibility of the constructed aircraft is tested and confirmed with real flight missions.

11.1 Introduction

With more requirements imposed on unmanned aerial vehicle (UAV) for military tasks of surveillance, reconnaissance, and detecting in obstacle-rich areas, clandestine military bases, radiant areas, and other dangerous regions, the desire and interest in research of micro aerial vehicle (MAV), or even nano aerial vehicle (NAV), are aroused (Wang et al. 2011). These requirements involve higher intelligence for simultaneous localization and mapping (SLAM), path planning, and obstacle avoidance, along with battery technology to maintain long endurance flight and communication with the ground control station (Achtelik et al. 2009; Eresen et al. 2012; Meier et al. 2011; Phang et al. 2010). In the recent few decades, the development of integrated circuits and micro-electromechanical systems (MEMS) triggered the emergence of smaller and lighter electronics and mechanical systems. It provides the possibility to shrink the size and weight of the UAV to a new milestone.

In 1997, the Defense Advanced Research Projects Agency (DARPA) sets an official definition for MAV, which requires maximum dimension of the aircraft in any direction to be no greater than 15 cm and that the gross takeoff weight should not exceed 100 g, with up to 20 g devoted to payload. Based on these requirements, many UAV research groups initiated their MAV study with different design approaches, including fixed-wing, rotary-wing, flapping-wing, and other unconventional platforms (Al-Qadi et al. 2006; Michelson 2010; Petricca et al. 2011). One good example would be the Black Widow, an 80 g fixed-wing MAV developed by AeroVironment, which has a 15 cm wingspan and is claimed to be fully autonomous (Grasmeyer and Keennon 2011). It is, however, difficult for the fixed-wing platform to show its capability in indoor environments or cluttered outdoor environments such as forest and urban environment full of building and other obstacles, due to its limitation of hovering and vertically taking off and landing (VTOL) ability. Flapping-wing is a promising platform with its VTOL and hovering capabilities like that of an insect or a bird. In 2007, a 3 cm size flapping-wing MAV was developed by Harvard University, biologically mimicking the dipteran insects (Wood 2007). Unfortunately, there is no mature development of autonomous flapping-wing platforms due to the sophisticated flapping mechanism and wing structure aerodynamic analysis. Ducted-fan platform is also a possible approach for miniature aerial vehicle. A 150 g ducted-fan platform was developed by University of Bologna. This platform requires extra fins to control its attitudes, resulting in a large takeoff weight (Naldi et al. 2010).

Recently, due to its extreme stability and mechanical simplicity, quadrotor platforms have aroused the research interests of many researchers. There are, however, not many quadrotor MAV platforms lower than 50 g capable of autonomous flight. A research group from Stanford University has developed a micro quadrotor "Mesicopter", with an impressive weight of 3 g. It is, however, unable to take off due to its rotor efficiency problem (Kroo and Kuns 2001). Mellinger and his collaborators from GRASP lab have been working on the formation flight of quadrotor MAVs weighing 60 g each and have achieved impressive results (Mellinger et al. 2010, 2012). From the perspective of the platform approach, rotary-wing platforms, especially in the form of quadrotor, have the advantages in maneuverability and mechanical feasibility.

In this chapter, a guideline to design a micro aerial quadrotor vehicle, or in short quadrotor MAV, with the following specifications will be presented:

1. Target weight not higher than 50 g
2. Largest dimension smaller than 15 cm in any direction
3. Flight duration of 8 min

Systematic design procedures with scopes of the design blueprint in virtual 3D environment, functionalities analysis in simulations, hardware selection and avionic system design, electrical circuit and software debugging, mathematical modeling and parameters identification, model simulation and verification, as well as aircraft orientation control with real flight test will be discussed in detail. In regard to this work, great effort was made to investigate the feasibility of overall structure and to evaluate the platform from the aspects of weight, size, and power consumption with both experiments and simulations before manufacturing, which guarantees a flyable and stable platform.

Main contents of this chapter are divided into five sections. Section 11.2 is the virtual design of the overall platform, with respect to mechanical structure and natural frequency analysis. Section 11.3 describes the hardware selection and avionic design procedures. Section 11.4 is the nonlinear mathematics model derivation concerning the aspects of kinematics, rigid body dynamics, and motor dynamics, followed by parameters identification methods and controller design. In Sect. 11.5, real flight test data is used to verify the mathematical model and control laws.

11.2 Virtual Design Environment

Before constructing the quadrotor platform, the design was done in virtual design environments. Differing from the usual UAV in larger scale, the natural modes of the structure or platform play an important role in determining the stability of the quadrotor MAV. As the aircraft gets smaller and lighter, the effect of its vibration due to natural modes is disastrous. Therefore in this section, two design processes in developing small-scale quadrotor MAV are proposed to systematically determine the optimum shape for the platform, in terms of lightweight and natural mode avoidance.

The first process is to perform finite element analysis (FEA) on various platform shapes. FEA is a numerical approach in solving structural problems by discretizing

the problem where the domain to be analyzed is divided into a number of discrete elements. Using this approach, it offers great flexibility to model complex geometries which would be near impossible if analytical approach is taken. By undergoing FEA, the natural modes and frequencies of the platform can be estimated numerically. With this, a best possible candidate can be chosen from among the designs.

Upon obtaining an optimum structural shape of the platform according to the FEA results, the platform of the quadrotor MAV can then be designed with a 3D simulation software, where each individual part of the aircraft could be assembled in the software for an overall design. An advantage of utilizing simulation software is that it could estimate various important parameters of the designed aircraft, such as the weight, density, and the moment of inertia, in a way that the design could be customized freely in order to meet their requirements before they are fabricated to real physical objects.

11.2.1 MSC Patran and Nastran

MSC Nastran, one of the most widely used FEA commercial software, is utilized in simulating the vibration properties of the quadrotor MAV. It is a useful tool which simulates static and dynamic cases for a wide variety of complicated structural problems. In addition to Nastran, a modeler software called Patran is employed for finite element modeling. Patran provides geometry modeling, meshing, boundary condition, and material properties set up for Nastran. It is also used for postprocessing purpose. Provided in Nastran, Lanczos (1950) method is utilized for eigenvalue and eigenvector extraction purpose.

To investigate and design the quadrotor platform, single arm and full quadrotor models are constructed in Patran with the properties of carbon fiber composite material assigned to the software. The model is then fetched to Nastran to investigate its structural resonance. In corresponding specifically to the design of micro aerial quadrotor, the study is concentrated on natural mode analysis to determine the natural frequencies and mode shapes of the model. The natural mode analysis predicts the resonance for the structure and the type of resonance. On the other hand, the displacement response of the model can be determined using frequency response analysis when external steady-state oscillatory excitation (simulating rotor rotation) is applied.

11.2.1.1 Single Quadrotor Arm

A quadrotor consists of four extended arms attached to a body which holds the onboard electronics. The aim of carrying out the single quadrotor arm analysis is to provide a useful summary on the performance of different quadrotor arm shapes, and then among the few possible candidates under the constrained of weight and size, a best solution in terms of shape, length, and dimension can be obtained. In this analysis, the quadrotor arm is approximated as a cantilever beam which has a fixed end and a free end.

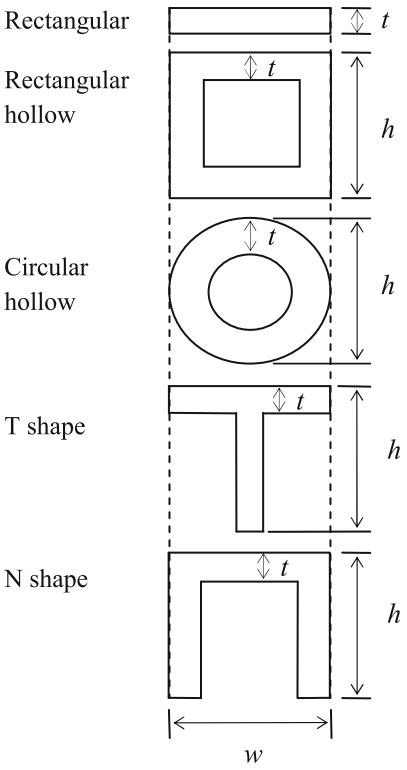

Fig. 11.1 Cross sections of five common beams

Five different types of cantilever beams are designed and analyzed. The cross sections for each of the beams are shown in Fig. 11.1. A few different parameters on the dimension of the beams will be varied, and the corresponding natural mode (1–4) will be compared. Note that the composite material for all beams to be simulated has the properties of carbon fiber code name carbon/epoxy T300/976. All simulations are done in Nastran by employing the discrete element with six degrees of freedom (DOF) per node, and all nodes at one of the tips are assumed to be fixed by setting all six DOF to zero.

The first variable to be investigated is the length of the beam. It is well known that slender bodies are more easily exposed to vibration, or in other words, shorter beams are stiffer. To verify the relationship between the length of the beam and its natural modes, the rectangular beam (first cross section in Fig. 11.1) with different length is analyzed in the simulation. In Table 11.1, a summary of the Nastran natural mode analysis results obtained for this study is given. Based on the results, it is evident that natural frequencies for the first four modes increase as the structure becomes shorter. In general, beams of other shape show similar behavior, and thus the results are trivial and not to be included here. Despite the results favoring shorter beams, there are other restrictions on the minimum length of the quadrotor arms. One important factor would be the aerodynamic interferences between the rotors, which generally limits the minimum length of the quadrotor arms to be at least twice the rotor radius.

Table 11.1 Natural frequencies of thin plate with varying length

Length (mm)	Natural frequency (Hz)			
	Mode 1	Mode 2	Mode 3	Mode 4
50	614.6	3, 656.7	3, 803.4	10, 518
60	426.85	2, 546.1	2, 642.6	7, 313.4
70	313.62	1, 873.6	1, 942.1	5, 377.1
80	240.3	1, 437.1	1, 491.3	4, 137.1
90	189.73	1, 135.4	1, 175.3	3, 255.4
100	153.68	920.14	952.05	2, 637.5

Table 11.2 Natural frequencies of beam with different cross sections and thickness

	1 mm thickness		0.5 mm thickness	
Type of cross section	Weight (g)	Mode 1 (Hz)	Weight (g)	Mode 1 (Hz)
Rectangular	0.5328	426.85	0.2664	213.45
Rectangular hollow	1.776	3,032.4	0.9768	3,270.7
Circular hollow	1.3949	2,647.9	0.767	2,851.6
T shape	0.9768	1,902.8	0.5106	1,845.3
N shape	1.4208	2,717.5	0.7548	2,810.4

The second variable to be investigated is the thickness of the material. As two common thickness of carbon fiber sheet or beam available commercially are of 0.5 and 1 mm thick, the natural mode of all five general shapes of beams are analyzed and compared in 0.5 and 1 mm thickness. For fair comparison, the model for each cross section was constructed with length $l = 60$ mm, width $w = 6$ mm, and height $h = 6$ mm (see Fig. 11.1 for illustration). Table 11.2 shows the comparison between beam with thickness $t = 1$ mm and $t = 0.5$ mm, together with their calculated weight. One can notice that in general, the beam having a closed cross-sectional shape, i.e., the rectangular hollow and circular hollow beams, has a much higher natural frequency compared to other shapes. Also, the thickness of the material has little effect on them, while the weight could be half as light.

The last variable to be investigated is the width and height of these closed cross-sectional beams. It can be seen from Table 11.3 that the height variation of the rectangular hollow beam affects the first mode frequency more severely than the second mode frequency. On the other hand, the width variation of the beam affects the second mode frequency much more than the first mode frequency. In conclusion, utilizing a square beam with equal height and width will give similar frequencies for the first and second modes. This is further proven in Table 11.4 where the circular hollow beams were analyzed.

In general, although the rectangular solid and T-shape configurations show better weight budget, their natural frequencies are comparatively much lower than that of rectangular hollow and circular hollow shapes, which are in the closed cross section forms. In the following section, a full quadrotor configuration with rectangular hollow beam of 3 mm height and 3 mm width will be investigated.

Table 11.3 Natural frequencies of the rectangular hollow beam with different width and height (0.5 mm thickness)

Height (mm)	Width (mm)	Natural frequency (Hz)			
		Mode 1	Mode 2	Mode 3	Mode 4
3	5	1,625.9	2,515.8	9,673.4	14,904
3	6	1,651.8	2,979.7	9,718.5	17,415
3	7	1,670.3	3,430.8	9,708.0	19,762
3	8	1,683.5	3,871.3	9,656.9	21,954
3	9	1,693.0	4,302.7	9,576.0	23,571
3	10	1,699.4	4,725.6	9,472.4	22,983
4	6	2,218.0	3,105.6	12,845	17,908
5	6	2,756.0	3,199.4	15,699	18,185
6	6	3,270.7	3,270.7	18,312	18,312

Table 11.4 Natural frequencies of the circular hollow beam with different radius (0.5 mm thickness)

Radius (mm)	Natural frequency (Hz)			
	Mode 1	Mode 2	Mode 3	Mode 4
2.0	1,839.3	1,839.3	11,070	11,070
2.5	2,347.5	2,347.5	13,875	13,875
3.0	2,851.6	2,851.6	16,495	16,495
3.5	3,349.6	3,349.6	18,911	18,911
4.0	3,840.1	3,840.1	21,117	21,117
4.5	4,322	4,322	23,116	23,116
5.0	4,794.3	4,794.3	24,918	24,918
5.5	5,256.1	5,256.1	26,538	26,538

11.2.1.2 Full Quadrotor Configuration

Due to structure stability shown by closed shape beams, the full configuration is then tested using rectangular hollow beam and circular hollow beam to form the arms attached to each corner of the main frame. The main frame is designed to be 28.28×28.28 mm with thickness 2 mm. Meanwhile, 60 mm long beam is employed as the quadrotor arm. Again, unidirectional carbon/epoxy T300/976 is used. In Patran, the main frame is modeled as 2-D shell element while the quadrotor arm using 1-D beam.

For this analysis, the main frame is assumed to be rigid and thus fixed in all three translation DOF. For a quadrotor model with 3 mm width, 3 mm height, and 1 mm thickness rectangular hollow beam, the resulted natural frequency for the first and second modes are 971.92 and 5,843.3 Hz. On the other hand, the natural frequency for quadrotor model using circular hollow beam with outer diameter of 3 mm and thickness of 1 mm is at 940.35 Hz for the first mode and 5,070.7 Hz for second mode.

Subsequently, dynamic analysis is performed to investigate the response of the quadrotor to oscillatory excitation produced by the propeller blades. In this simulation, a 0.25 N oscillatory force is applied to the tip of each quadrotor arms. The analysis is performed over frequency range of 0–4,000 Hz. Results obtained from the Nastran are displayed in Fig. 11.2a, b. From the response spectrum, the frequency at peak for both quadrotor models matches the first natural mode

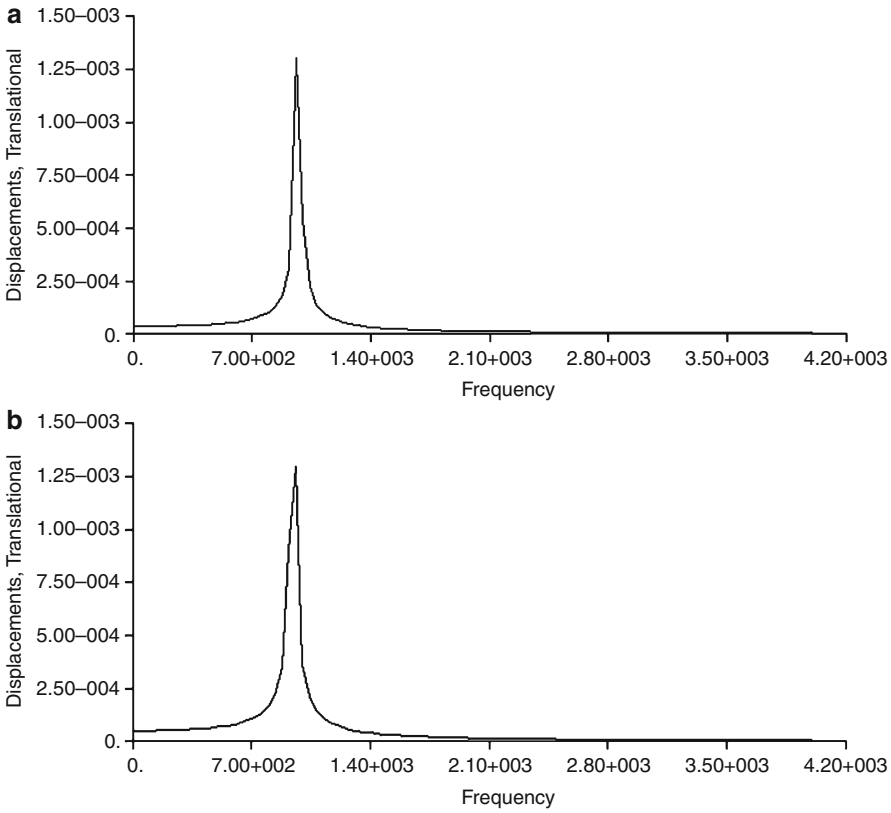

Fig. 11.2 Displacement at tip of the arm with rectangular (**a**) and circular (**b**) hollow beam

simulated earlier. Based on the simulation result, both models are suitable for miniature quadrotor design as they have the highest stiffness to weight ratio among the tested shapes. In conclusion, using a beam with a closed cross-sectional shape as the quadrotor arm can guarantee extreme stability for the whole quadrotor model.

11.2.2 SolidWorks

An overall design blueprint of this quadrotor platform is essential to provide a broad overview of the quadrotor functionalities, size, weight, and appearance design. A 3D mechanical design software named SolidWorks, developed for efficient and quicker design of mechanical products and components, facilitates the design tasks for the platform. This 3D software is chosen as the design and analyzing software over other mechanical design tools due to a few advantages, such as increase design efficiency, ease of fabricating, and easy access to simulated geometric data.

Table 11.5 Weight budget for quadrotor MAV

Components	Amount	Estimate weight (g)	Current weight (g)
Battery	1	10	9.8
Motor and propeller	4	3.5	3.59
Quadrotor arm	4	1	0.93
Quadrotor frame	1	4	2.13
Onboard system	1	10	7.32
Miscellaneous		2	1.7
Total		44	39.03

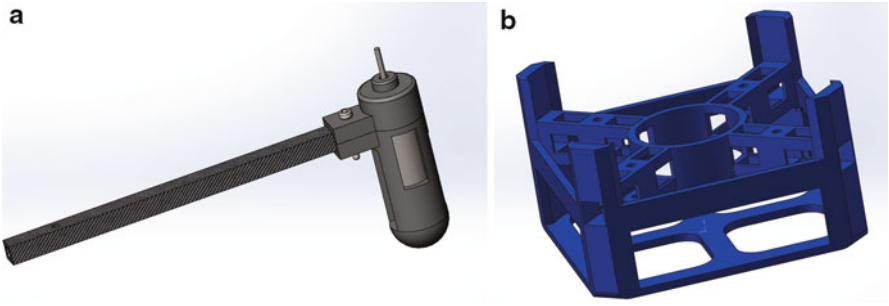

Fig. 11.3 Quadrotor arm and frame design in SolidWorks

Based on the natural mode analysis in Nastran (see previous section), a cross-shaped frame structure is designed with four rectangular hollow carbon fiber beams fixed into a holder locating the avionic system along with the battery. The design takes the following considerations:

1. The CG should be located on the z-axis at the geometrical center of the cross shape.
2. Mechanical parts should be carefully designed with the weight and moment of inertia symmetrically distributed along the x- and y-axis.
3. Materials with low density and high intensity are to be used as the frame and protection to satisfy weight limit.

In order to accurately approximate the weight and dimension of the overall design, components are to be drawn on scale, with the correct weight and density assigned to it in SolidWorks. As weight is the main constraint to the design of the MAV, the design parts are minimized. Table 11.5 details the total parts in the design of the quadrotor MAV, with specific weight budget assigned to each of them. On the right of the table listed the real weight of the components or designed parts, which will be detailed here and also in the next sections.

The structure design can be separated into two different parts:

1. *Quadrotor arms*: A protection scheme is developed as a shell to encapsulate the motor into a tight chamber to fix its position. Carbon fiber beam can be mounted and screwed to the side, as shown in Fig. 11.3a.

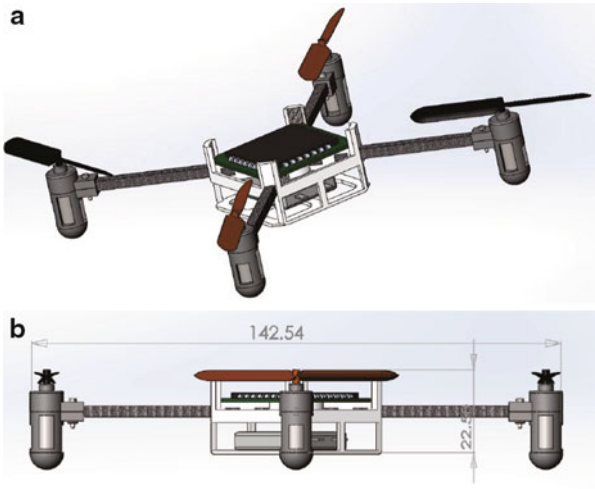

Fig. 11.4 Mechanical structure layout and size of the quadrotor

2. *Main body*: The main frame structure has four slots for the quadrotor arms and contains two layers, where the avionic system is placed on the top and the battery is located in the lower level, as shown in Fig. 11.3b. It is fabricated with acrylonitrile butadiene styrene (ABS).

The mechanical structure layout of the proposed quadrotor MAV is shown in Fig. 11.4a with all the parts assembled together as shown in Fig. 11.4b. Distance of two diagonal rotors is 142.54 mm, with a total height of 22.50 mm. Details of weight breakdown are reflected in Table 11.5. In this table, the estimated weight is approximated based on the design guideline shown in this chapter, while the current weight on the right of the table is the measured weight of the quadrotor MAV prototype, code name KayLion, made by National University of Singapore, following the guideline.

11.3 Hardware Design

Hardware system and the avionics are the core of any unmanned aircraft design. The hardware system includes the motors and propellers, avionics such as onboard processor (CPU), sensors like inertial measurement unit (IMU), and power supply. Suitable choices of the hardware and components will be proposed based on the requirement on their performance under the constraint on weight and size.

11.3.1 Motor and Propeller

Motor and propeller sets are the main actuators of the quadrotor MAV. As each quadrotor consists of four sets of motor and propeller, they need to be chosen carefully as their characteristics must satisfy the design requirements. A few

important design requirements of the quadrotor MAV are directly related to the characteristic of the motor and propeller. They are the operation voltage and current consumption of the motors, the weight of the motors, and the maximum thrust it can produce with different propellers.

Based on the requirements stated above, a 8,000 kV single cell brushed direct current (DC) motor is utilized. Combined with two sets of propeller, each has a clockwise and an anticlockwise propellers; the total weight of a single motor and propeller is approximately 4 g. Test bench experiment has proved that the combination could produce a maximum thrust of 16 g each, which combined to be approximately 1.5 times larger than the proposed MAV at 40 g.

11.3.2 Electronics

The avionic system consists of electronic components for the electrical system of the quadrotor MAV. Different from the conventional design of the avionic system for larger UAV, where each component can be chosen from the commercially off-the-shelf (COTS) product, with firm packaging and plug-and-play connection ready, the choices of electronic components for the quadrotor MAV need to be made down to integrated chip (IC) level. A printed circuit board (PCB) incorporated all onboard electronics will then be designed.

11.3.2.1 Control CPU

The processor is the core of the avionic system. In the compact MAV design, the main tasks of the processor are (1) collecting data from IMU sensor from serial port, (2) receiving command from the receiver in the form of pulse position modulation (PPM) signal, (3) decoding and analyzing data, (4) realizing flight control laws, (5) sending control signals in the form of pulse width modulation (PWM) signal to the electronic speed controllers (ESC), and (6) sending logging data to the logger via serial port.

For the selection of the microprocessor for the abovementioned tasks, ATmega328P, a high-performance Atmel 8-bit AVR RISC-based microcontroller, is adopted because of the following features: (1) availability of various ports, such as UART, SPI, and PWM ports; (2) low power consumption; and (3) ease of coding.

It is proved that the ATmega328P microprocessor is good enough to run the software for the tasks mentioned above within 5 ms. As a result, the control loop running in the software is user configurable up to 200 Hz, depending on the update frequency of the IMU sensor.

11.3.2.2 Inertial Measurement Unit

An IMU is an essential sensor to any autonomous aircraft. It provides important motion measurements of the body it attached to, such as accelerations, angular rates, and magnetic values. It is noted that for most of the aircraft orientation control, 3-axis Euler angle measurements must be provided. However, it is not necessary that all IMU provides the angular measurements as they can be estimated by using an extended Kalman filter (EKF) (Jang and Liccardo 2007) or complimentary

filtering (Yun et al. 2007). These filters are, however, computationally intensive; thus, they might be a burden for the onboard AVR microprocessor. Here, a solution is to find a powerful IMU with in-built EKF algorithm in a small and light package.

The VN-100 SMD from VectorNAV is chosen in the design. It is a lightweight (3 g) and miniature (24 × 22 × 3 mm) high-performance IMU and Attitude Heading Reference System (AHRS). In this tiny package, it includes 3-axis accelerometer, 3-axis gyroscope, and a 3-axis magnetic sensor. An extra advantage of VN-100 is the in-built 32-bit microprocessor to compute and output a real-time and drift-free 3D orientation solution with EKF algorithm. The IMU output rate is user-configurable from 40 to 200 Hz, depending on the output methods.

11.3.2.3 Motor Speed Controller

ESC is essential for each brushed motor used in the MAV design. The main contribution of ESC is to convert the commonly used PWM signal to analog signal to be fed to the motor. The current of the analog signal will be further boosted to drive the motor. For the ESC design, a single 8-pin processor ATtiny13A is utilized for speed controlling. The processor is responsible for decoding PWM signals fed from the control CPU (ATmega328P) and outputting a stable analog voltage. The current output of the analog port is, however, too low to drive the motor. Thus a single MOSFET chip is also included to feed the current from the aircraft's power supply (battery) directly to the motor. Four ESCs and MOSFETs are needed for the quadrotor MAV design.

11.3.2.4 Radio-Frequency Receiver

Conventionally, a radio-frequency (RF) receiver is used to receive and decode RF signals sent from a transmitter controlled by a ground pilot in radio-controlled (RC) flights. In general, a receiver is not needed in a fully autonomous flight control system as no remote pilot is needed. Most of the UAV designs, however, retain the receiver component for fail-safe purposes, where a ground pilot has higher authority to remotely control the UAV during emergencies such as controller failures. In the quadrotor MAV design, the receiver has a different function. Besides receiving the control signals from the remote pilot, the receiver is utilized to receive control signals or measurement values from the ground control station in autonomous mode. It is particularly useful when the MAV system is navigating in indoor environment with the aid of VICON motion technology, where the VICON system measures the position and velocity of the MAV, then sends the control signals or the measurement values to the aircraft's onboard CPU via the transmitter to receiver link. This communication system could be realized with a PCTx cable, a product by Endurance R/C. The PCTx cable connects the ground station (desktop or laptop) to the transmitter, making use of the transmitter to send RF signals to the onboard receiver. Upon receiving signals from the ground, the receiver will then output the signals in the form of PPM signal to the onboard CPU for processing. In order to fulfill the mentioned requirement, a good candidate would be Rx31d from DelTang. It is chosen to be integrated in the avionic system due to its ultra tiny package of 10 × 10 mm with 0.21 g. It is able to provide up to seven channels of PPM signals.

11.3.2.5 Data Logger

In most UAV designs, important flight data such as state variables of the UAV model will be recorded for post-flight observation and investigation. In the design of the MAV, a logger is required to be small, light, and simple enough to work. An open source data logger, called OpenLog from SparkFun, is utilized in the design. OpenLog is presented in a tiny package with 1.70 g. It will start logging any serial data up to 115,200 baud rate to the micro SD card upon powered up. Optionally, as SparkFun provides OpenLog firmware and design files, it can be redesigned to the main PCB of the MAV.

11.3.3 Power Supply

The main consideration in designing the power supply is to meet the overall system and flight duration requirements. The choice of power supply is important as it constitutes most (approx. 30 %) of the overall weight of the MAV, and the power needed to lift the MAV will be increased due to its own weight. As all onboard components can be powered up with 3.3 V, a single cell Lithium-Polymer (Li-Po) battery with current capacity of 360 mAh is utilized to power the avionics and to drive the motors. A 3.3 V regulator is included to provide a clean voltage to the components, as single cell Li-Po battery's output varied from 4.2 V during full charged down to lower than 3.4 V when it is used up. The battery is as light as 10 g and is able to provide enough energy for an 8-min flight duration.

11.3.4 Avionics Design

In this subsection, the design process of the PCB for the avionic system of the quadrotor MAV will be described in detail. Among the five components to be included to the avionic system, the IMU, flight control CPU, and four ESCs will be incorporated into the design, while the receiver and the logger will be attached to the designed PCB. A general guideline to design avionics PCB for quadrotor MAV with Altium Designer is as follows:

1. *Schematic design* – A schematic diagram of the design must be drawn in Altium Designer with all the components needed, including four status indication LEDs. A 3.3 V voltage regulator is also included.
2. *Layout assignment* – The layout of the components of the PCB is important so as to reduce the electromagnetic interference between the components. To satisfy the dimension and weight constraints, a maximum of 4×4 cm PCB layout is imposed. The IMU must be placed in the middle of the design to be as closed to the CG as possible with the correct orientation. Then, components such as flight control CPU and motor speed controllers are placed at the opposite side of the board. Lastly, the four LEDs are located in a way that they are clearly visible to the user during flight.
3. *Routing* – The final step of designing PCB is the routing to connect each component according to the connection assigned in the schematic phase. The routing could be easily done (see Fig. 11.5) in a 2-layer-PCB setup.

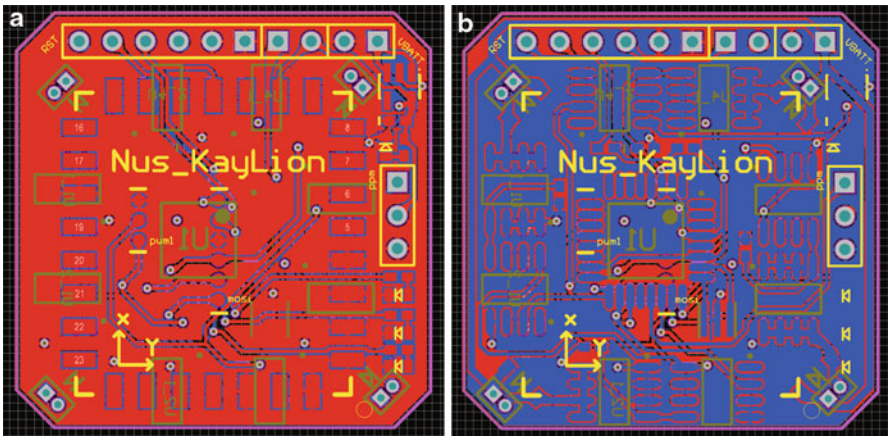

Fig. 11.5 PCB layout

Once the design is done, it can be sent to PCB manufacturer to fabricate. With PCB thickness of 1 mm, the fabricated product is approximately 7 g including all components, within the dimension of $40 \times 40 \times 1$ mm.

11.4 Dynamic Modeling and Control

In this section, a nonlinear mathematic model of the quadrotor MAV is derived. The methods of parameters identification will also be discussed, which include direct measurement, test bench experiments, as well as evaluation in virtual environment. This mathematic model is further verified with the real flight test data obtained by the VICON motion capture system. PID control law is first implemented in the virtual model in Simulink, then further fine-tuned on the real platform based on the flight tests.

11.4.1 Nonlinear Mathematics Model

The mathematical models of quadrotor aircraft are quite well developed in the literature (Bouabdallah et al. 2004; Erginer and Altug 2007; Guerrero-Castellanos et al. 2011; Kim et al. 2007; Phang et al. 2012; Pounds et al. 2006). The overall structure view of this quadrotor platform is pictured in Fig. 11.6, where δ_{ail}, δ_{ele}, δ_{thr}, and δ_{rud} represent the normalized input signals from aileron, elevator, throttle, and rudder channels, respectively. δ_1, δ_2, δ_3, and δ_4 are the normalized input values to each motors. Ω_1, Ω_2, Ω_3, and Ω_4 are motors' individual rotational speeds. Linear velocity u, v, w and angular velocity p, q, r can be obtained by 6 degree-of-freedom (DOF) rigid body dynamics, and position in ground frame x, y, z and Euler angles ϕ, θ, ψ can be calculated through kinematics equation.

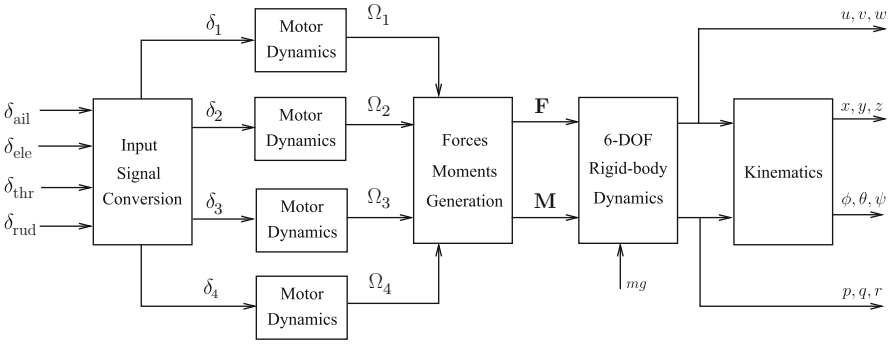

Fig. 11.6 Overall structure of the quadrotor

Two coordinate frames, north-east-down (NED) frame $[x_i \ y_i \ z_i]$ and the body frame $[x_b \ y_b \ z_b]$, will be considered (Wang et al. 2012). The NED frame is stationary with respect to a static observer on the ground, and the body frame is the coordinate frame with the origin located at the CG and orientation moving together with the aircraft fuselage. The origin of the body frame is located at the CG of the platform with x-axis parallel with rotor 2 and rotor 3 along with y-axis parallel with rotor 1 and rotor 2. Euler angles $\Theta = [\phi \ \theta \ \psi]^T$ are the angles rotating about x-, y-, and z-axis, describing the roll, pitch, and yaw motions. T_1, T_2, T_3, and T_4 are the lift force created by rotor 1, 2, 3, and 4. Rotors 1 and 3 rotate clockwise, while rotors 2 and 4 rotate counterclockwise.

11.4.1.1 Kinematics and 6 Degree-of-Freedom Rigid Body Dynamics

At any time instant, the aircraft can be pictured as having a translational and rotational motion with respect to the stationary NED (or ground) frame. The following kinematics equations represent the navigation equations applicable to transformation between the two frames:

$$\dot{\mathbf{P}}_\mathbf{n} = \mathbf{R}_{\mathbf{n/b}}\mathbf{V}_\mathbf{b}, \tag{11.1}$$

$$\dot{\Theta} = \mathbf{S}^{-1}\Omega, \tag{11.2}$$

where $\mathbf{R}_{\mathbf{n/b}}$ represents the transformation matrix and $\mathbf{S}^{-1}$ represents a lumped transformation matrix. They are given by:

$$\mathbf{R}_{\mathbf{n/b}} = \begin{bmatrix} c_\theta c_\psi & s_\phi s_\theta c_\psi - c_\phi s_\psi & c_\phi s_\theta c_\psi + s_\phi s_\psi \\ c_\theta s_\psi & s_\phi s_\theta s_\psi + c_\phi c_\psi & c_\phi s_\theta s_\psi - s_\phi c_\psi \\ -s_\theta & s_\phi c_\theta & c_\phi c_\theta \end{bmatrix}, \quad \mathbf{S}^{-1} = \begin{bmatrix} 1 & s_\phi t_\theta & c_\phi t_\theta \\ 0 & c_\phi & -s_\phi \\ 0 & s_\phi/c_\theta & c_\phi/c_\theta \end{bmatrix}, \tag{11.3}$$

with $s_* = \sin(*)$, $c_* = \cos(*)$, $t_* = \tan(*)$.

Based on Newton-Euler formalism describing the translational and rotational dynamics of a rigid body, the dynamic equations can be written into the following input-output form:

$$m\dot{\mathbf{V}}_\mathbf{b} + \Omega \times (m\mathbf{V}_\mathbf{b}) = \mathbf{F}, \tag{11.4}$$

$$\mathbf{J}\dot{\Omega} + \Omega \times (\mathbf{J}\Omega) = \mathbf{M}, \tag{11.5}$$

where $\mathbf{F}$ and $\mathbf{M}$ are the force and moment vectors, m is the mass of aircraft, and $\mathbf{J}$ is the tensor of inertia matrix.

11.4.1.2 Forces and Moments Generation

Based on the working principle of the quadrotor (Cai et al. 2011), the forces and torques are mainly generated by the four rotors (Goel et al. 2009). The following equation represents the component part of the overall force and moment vector:

$$\Lambda = \begin{bmatrix} \mathbf{F} \\ \mathbf{M} \end{bmatrix} = \begin{bmatrix} \mathbf{F}_g + \mathbf{F}_m \\ \mathbf{M}_m + \mathbf{M}_{gy} + \mathbf{M}_{rt} \end{bmatrix}, \tag{11.6}$$

where subscripts g, m, gy, and rt correspond to forces and moments generated by gravity, rotors, gyroscopic effect, and reactional torque, respectively.

As the platform is four-way symmetric, the CG is located on the z-axis, thereby the gravitational force only contributes to the force vector. Considering the coordinate frames, the gravity only exists on the z-axis in NED frame and needs to be transformed to the body frame by the transformation matrix:

$$\mathbf{F_g} = \mathbf{R_{n/b}}^{-1} \begin{bmatrix} 0 \\ 0 \\ mg \end{bmatrix} = \begin{bmatrix} -mgs_\theta \\ mgc_\theta s_\phi \\ mgc_\theta c_\phi \end{bmatrix}. \tag{11.7}$$

It is the motor and propeller pairs which produce the main movements to generate the forces and moments. As in Pounds et al. (2004), let T_i and Q_i be the thrust and torque created by i-th rotors ($i = 1, 2, 3, 4$); they can be expressed as below:

$$T_i = C_T \rho A (\Omega_i R)^2, \tag{11.8}$$

$$Q_i = C_Q \rho A (\Omega_i R)^2 R, \tag{11.9}$$

where C_T and C_Q are the propeller aerodynamic coefficient, ρ is the air density, A is the area of the propeller swept by the rotating rotor, and R is the radius of the rotor A. Assuming that the distortion of the propellers during high frequency rotation can be ignored, Eqs. (11.8) and (11.9) can be simplified as:

$$T_i = k_T \Omega_i^2, \tag{11.10}$$

$$Q_i = k_Q \Omega_i^2, \tag{11.11}$$

where these two coefficients k_T and k_Q can be obtained by a series of experiments. Thereby, the sum of these four thrusts will result in a total thrust in negative z-axis in the body frame, as below:

$$\mathbf{F_m} = \begin{bmatrix} 0 \\ 0 \\ -(T_1 + T_2 + T_3 + T_4) \end{bmatrix}. \tag{11.12}$$

The moments are generated when the four thrusts have different magnitudes, results in pitch, roll, and yaw movements, as shown below:

$$\mathbf{M_m} = \begin{bmatrix} \frac{\sqrt{2}}{2} l(T_2 + T_3 - T_1 - T_4) \\ \frac{\sqrt{2}}{2} l(T_1 + T_2 - T_3 - T_4) \\ Q_1 - Q_2 + Q_3 - Q_4 \end{bmatrix}, \tag{11.13}$$

where l is the distance from the center of the motor to the platform CG.

Gyroscopic effect is caused by the combinations of rotations of four propellers and can be modeled as

$$M_{gy} = \sum_{i=1}^{4} J_r \left(\Omega \times \begin{bmatrix} 0 \\ 0 \\ 1 \end{bmatrix} \right) (-1)^i \Omega_i \tag{11.14}$$

$$= \begin{bmatrix} -J_r q(\Omega_1 - \Omega_2 + \Omega_3 - \Omega_4) \\ J_r p(\Omega_1 - \Omega_2 + \Omega_3 - \Omega_4) \\ 0 \end{bmatrix} \tag{11.15}$$

where J_r is the moment inertia of the rotor, including the propeller and motor shaft. The gyroscopic effects produced by the propellers are only related to the moments of the aircraft.

The first-order derivative of rotational movement can cause the inertia counter torque, and this torque only affects the movement in yaw direction, which is

$$\mathbf{M_{rt}} = \begin{bmatrix} 0 \\ 0 \\ -J_r(\dot{\Omega}_1 - \dot{\Omega}_2 + \dot{\Omega}_3 - \dot{\Omega}_4) \end{bmatrix}. \tag{11.16}$$

11.4.1.3 Motor Dynamics

Each brushed motor is controlled by a single cell brushed ESC, and the steady-state value of rotor angular speed to brushed ESC input can be approximated as a linear

process near the equilibrium (hovering) value. The transient property of this brushed motor can be approximated as a first-order process, as shown below:

$$\dot{\Omega}_i = \frac{1}{T_m}[K_m(\delta_i - \delta_i^*) - \Omega_i], \tag{11.17}$$

where δ_i is the normalized input to the i-th motor, T_m and K_m are the time constant and process gain of the first-order model, and δ_i^* is the offset to the normalized input values. Note that the offset values of each motor are determined in the hovering condition.

11.4.2 Parameters Identification

Several parameters need to be identified to obtain the complete model. Here, several methods of identifying each parameters will be presented. They are all to be done by direct measurement, experiments, or computer simulation.

11.4.2.1 Direct Measurement

Parameters that can be directly measured by a weighing balance and ruler are mass of each components and the length of quadrotor arms, as follows:

$$m = 0.032\,\text{kg}, \tag{11.18}$$

$$L = 0.058\,\text{m}. \tag{11.19}$$

Gravitational acceleration, depends on the location, can be easily calculated given the latitude of the location. In Singapore in particular,

$$g \approx 9.781\,\text{m/s}^2. \tag{11.20}$$

11.4.2.2 Computer Simulation

Several parameters can be estimated numerically with computer software. As mentioned in the previous section, mechanical parts of the quadrotor MAV are first designed in SolidWorks, with exact density and scale to the real physical parts. A few parameters, such as the tensor moment of inertia of the quadrotor MAV and the rotating moment of inertia of the propeller, are calculated with the mass property function of SolidWorks:

$$J = \begin{bmatrix} 3.0738 & 0 & 0 \\ 0 & 3.0849 & 0 \\ 0 & 0 & 5.9680 \end{bmatrix} \times 10^{-5}\,\text{kg m}^2, \tag{11.21}$$

$$J_r = 5.897 \times 10^{-8}\,\text{kg m}^2. \tag{11.22}$$

Note that J is diagonal as the designed quadrotor structure is highly symmetric.

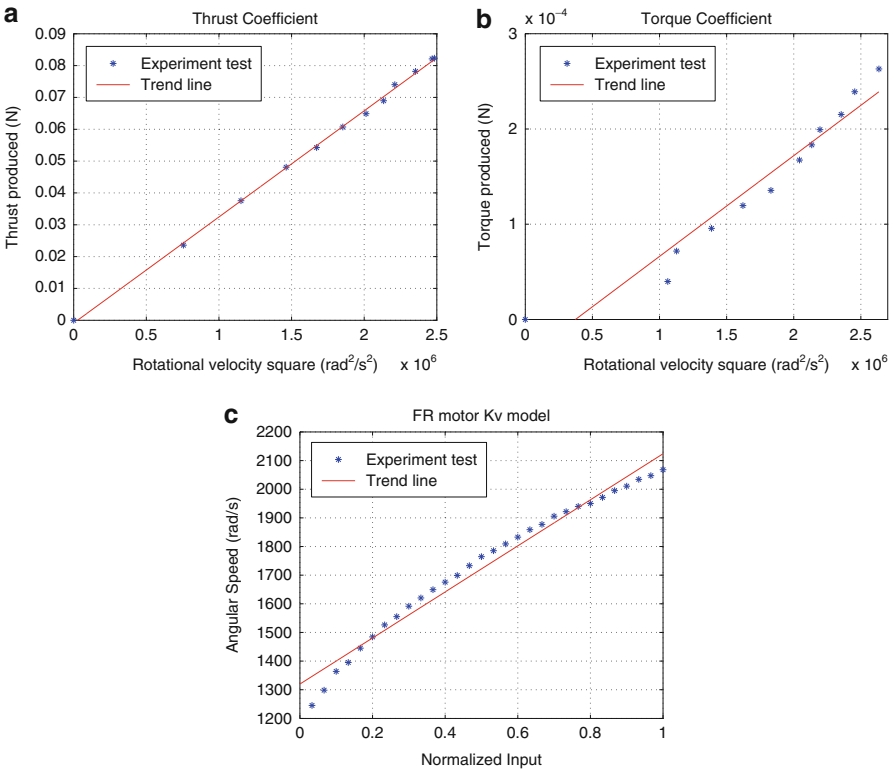

Fig. 11.7 Measurement of thrust coefficient, torque coefficient, and motor's steady-state gain

11.4.2.3 Test Bench Experiment

The thrust and torque coefficient of the rotor can be measured by lever-balance setup. An infrared transceiver is used to measure the time interval between two adjacent cutting of the propeller, where the real-time angular velocities can be calculated. Thrust and torque produced by the rotor can be measured from the weighing scale. The results are plotted in Fig. 11.7a, b. Thrust and torque coefficients k_T and k_Q can then be obtained as the gradient of the approximate line:

$$k_T = 3.334 \times 10^{-8}\,\mathrm{N/(rad^2/s^2)}, \tag{11.23}$$

$$k_Q = 1.058 \times 10^{-10}\,\mathrm{Nm/(rad^2/s^2)}. \tag{11.24}$$

The next experiment is conducted to estimate the brushed motor dynamics. Several different values of constant input are fed to the motor, and the resultant angular speeds of the motors are recorded with the similar setup as the experiment above. The results are plotted in Fig. 11.7c. Here the motor steady-state velocity is

assumed to be proportional to the input value at equilibrium (during hover). Thus, the steady-state gain, K_m, can be extracted as

$$K_m = 803.9. \tag{11.25}$$

Also, as presented in Eq. 11.17, the motor dynamics can be approximated as a first-order process:

$$\frac{\Omega_i(s)}{R_i(s)} = \frac{K_m}{T_m s + 1}, \tag{11.26}$$

where average time constant T_m is estimated from the transient response of a step input to the motor. The value obtained is

$$T_m = 0.0821\,\text{s}. \tag{11.27}$$

11.4.3 Controller Design

Upon obtaining the mathematical model of the aircraft, a simple yet reliable PID controller is designed and simulated with the aid of Simulink in MATLAB.

Generally, the dynamics of a quadrotor without orientation stabilizer is too fast even for a skilled human pilot. The fast dynamics is contributed by the roll and pitch movements, while the yaw movement exhibits much slower dynamics.

In the initial stage of the PID gains tuning, the controller is first designed in simulation by utilizing the Ziegler-Nichols method. Simulated result in Fig. 11.8 has shown a stable quadrotor system, with all the Euler angles, and angular rate signals are attenuated to zero within 5 s. This set of PID gains is further fine-tuned with real flight tests. Finally, a set of PID gains for each axis in which the aircraft is able to stabilize horizontally on this setup was obtained, as shown in Table 11.6.

11.5 Flight Test Results

The PID controller designed with software simulator shown above is implemented to the manufactured quadrotor MAV code-named KayLion (Fig. 11.9). Flight tests are then carried out to test the endurance of the vehicle and to verify the mathematical model derived in the previous section.

In particular, chirp-like oscillating inputs are sent to the MAV system, while its Euler angles and angular rates responses are recorded in the onboard logger. The recorded responses are then compared to the simulated responses by using

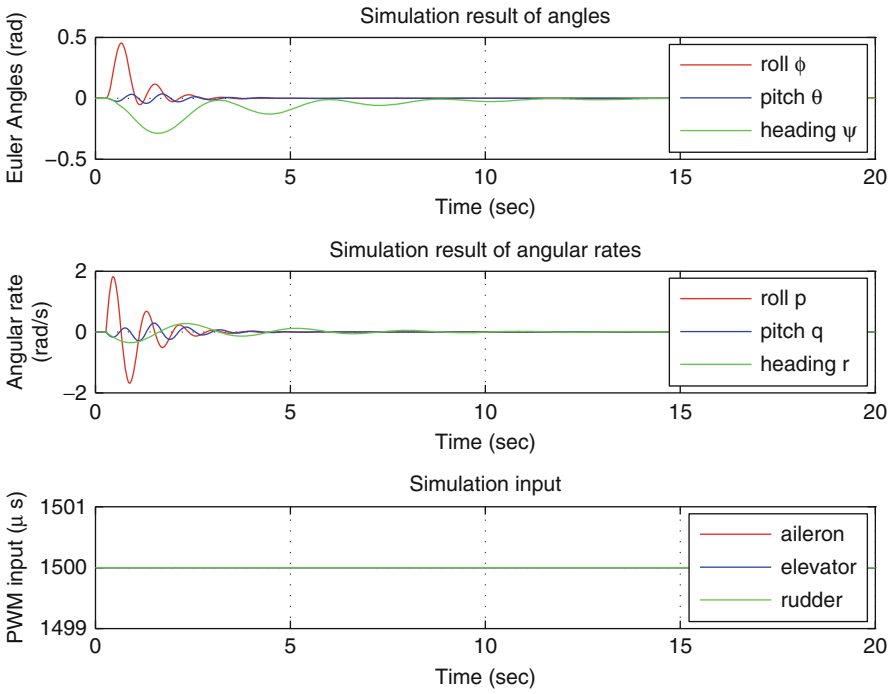

Fig. 11.8 Simulation results with PID gains

Table 11.6 PID gains implemented to the quadrotor MAV

Channel	K_p	K_i	K_d
Pitch	1.60	2.45	0.51
Roll	1.60	2.45	0.51
Yaw	4.00	0.75	0.10

the exact inputs to the simulator. Figure 11.10a shows the perturbation signal on elevator channel to the MAV, while Fig. 11.10b shows the responses of the system in pitch direction plotted together with the simulated results. Besides some random low-amplitude oscillations caused by the disturbances from the air movement, the responses match fairly well. Beside the pitch direction, the roll direction is assumed to be similar to the pitch, as the quadrotor MAV is of four-way symmetry.

In the other flight test, a chirp-like signal was injected to the throttle channel of the quadrotor MAV, resulting in agitated heave movement. In this experiment, a VICON Motion Tracking System is used to measure and compute the position of the quadrotor with reference to the start-up origin. Both the input signals and position measurement are logged and plotted in Fig. 11.11a, b. In the latter figure, it can be seen that the derived mathematical model on heave movement matches well with

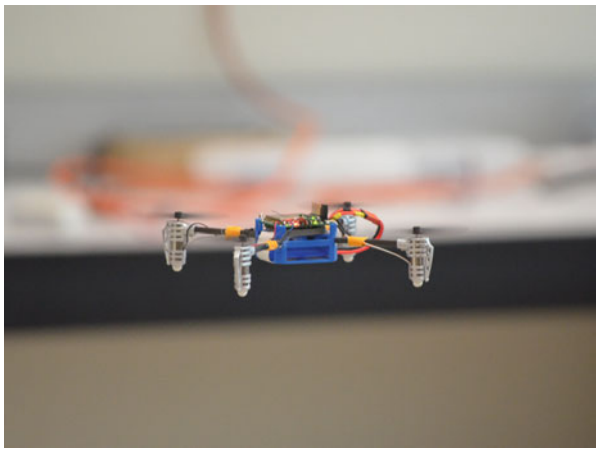

Fig. 11.9 A full working prototype quadrotor MAV, KayLion, designed and built by the National University of Singapore (NUS)

the experimental data to a certain perturbation frequency, which is approximately 1 Hz. The quadrotor MAV was unable to respond to the perturbation signal above this frequency, as it was observed with naked eyes during the flight tests.

11.6 Conclusions

This chapter summarizes the steps to design and implement a micro scale quadrotor MAV, with a target take-off weight of less than 50 g. It has covered the full design areas, including the structural design, platform design, avionics design, and controller design, in which all areas are supported and verified by simulation or experimental results.

Structural analysis was first done in MSC Patran and Nastran to obtain suitable candidates for the platform design, where the shape of the beam with the highest stiffness against weight ratio was selected. The platform including the arms was then designed in SolidWorks to ensure proper placement of components. Next, the avionic system design was discussed, first with the selection of suitable electronics and constraints to the trade-off between weight and performance, followed by a detailed guideline to integrate these components to a single PCB. Once the platform was fabricated, a nonlinear mathematical model of the quadrotor MAV was derived. PID controller was implemented to the quadrotor, and flight tests were done to fine-tune the controller.

The flight test results have verified the design of the quadrotor MAV, from structural development to the avionic system implementation, and it has further proven the accuracy of the derived mathematical model. With the availability of the mathematical model for this quadrotor MAV, it serves as a good platform to test and verify control law design and implementation.

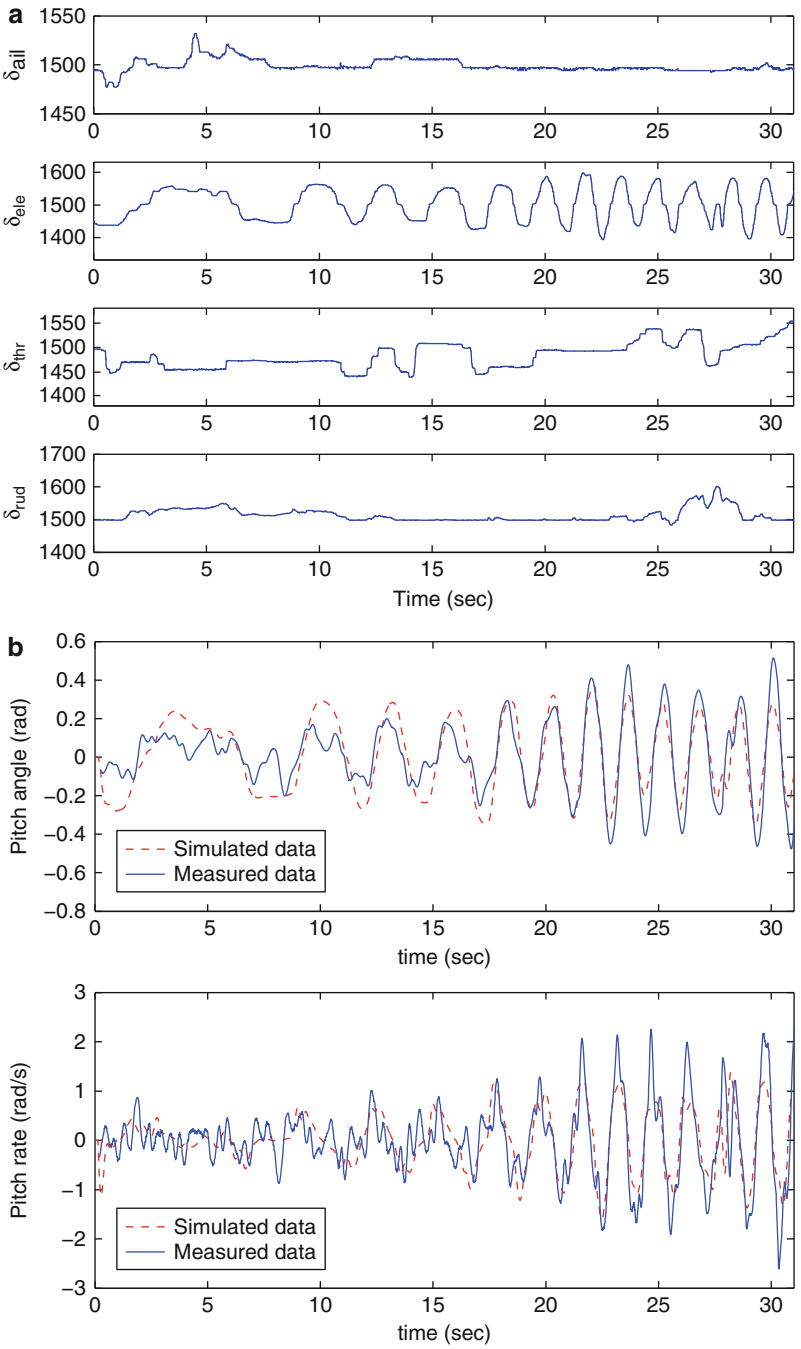

Fig. 11.10 Pitch angle and angular rate of the system response together with simulated response

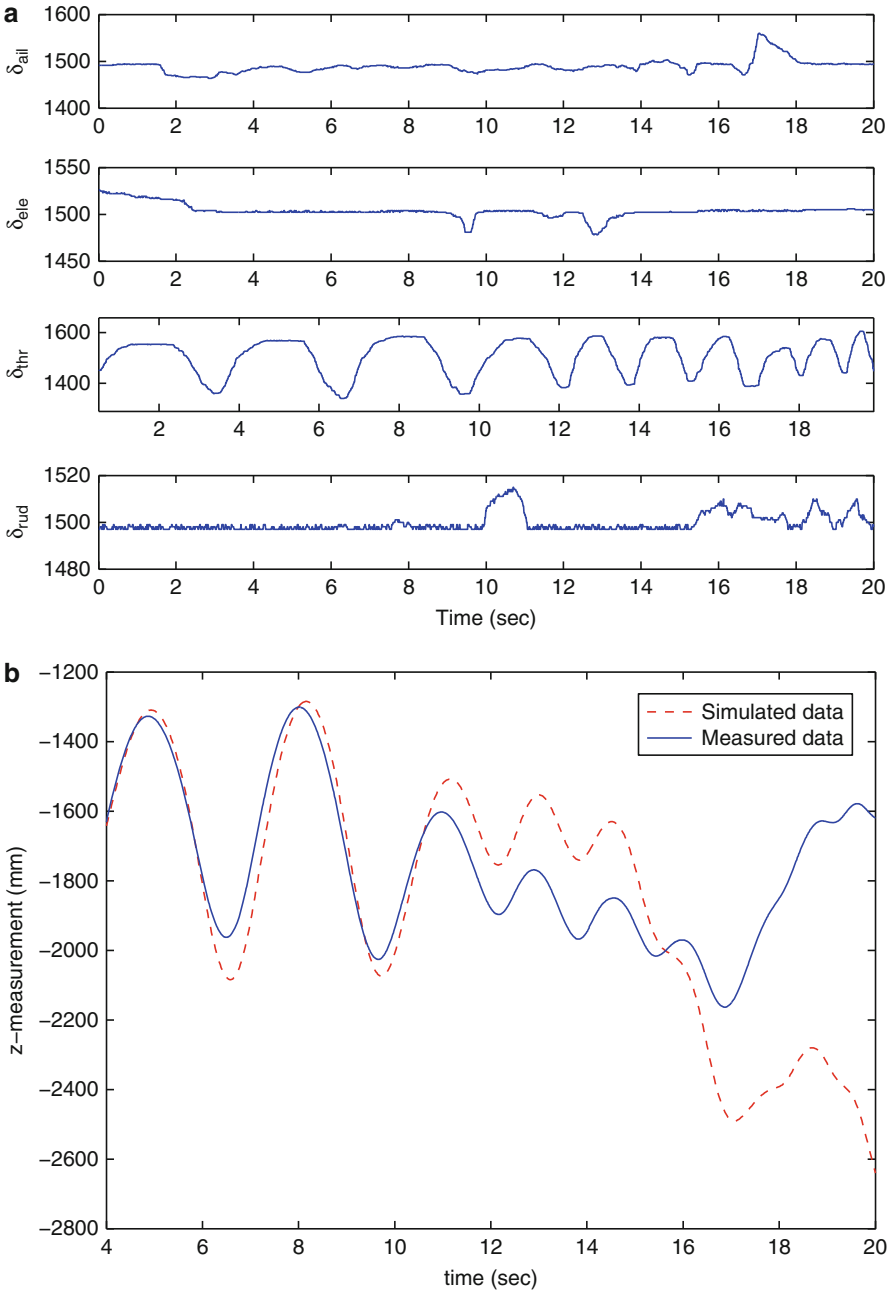

Fig. 11.11 z-axis position of the system response together with simulated response

References

M. Achtelik, A. Bachrach, R. He, S. Prentice, N. Roy, Autonomous navigation and exploration of a quadrotor helicopter in GPS-denied indoor environments, in *IEEE ICRA*, Kobe, 2009

M.I. Al-Qadi, A.M. Al-Bahi, Micro aerial vehicles design challenges: state of the art review, in *SSAS UAV Scientific Meeting & Exhibition*, Jeddah, 2006

S. Bouabdallah, A. Noth, R. Siegwart, PID vs LQR control techniques applied to an indoor micro quadrotor, in *IEEE International Conference on Intelligent Robots and Systems*, Sendai, 2004, pp. 2451–2456

G. Cai, B.M. Chen, T.H. Lee, *Unmanned Rotorcraft Systems* (Springer, London/New York, 2011)

A. Eresen, N. Imamoglu, M.O. Efe, Autonomous quadrotor flight with vision-based obstacle avoidance in virtual environment. Expert Syst. Appl. **39**(1), 894–905 (2012)

B. Erginer, E. Altug, Modeling and PD control of a quadrotor VTOL vehicle, in *IEEE Intelligent Vehicles Symposium*, Istanbul, June 2007

R. Goel, S.M. Shah, N.K. Gupta, N. Ananthkrishnan, Modeling, simulation and flight testing of an autonomous quadrotor, in *Proceedings of International Conference on Environmental and Agriculture Engineering*, Bangalore, 2009

J.M. Grasmeyer, M.T. Keennon, Development of the black widow micro air vehicle. Prog. Astronaut. Aeronaut. **195**, 519–35 (2011)

J.F. Guerrero-Castellanos, N. Marchand, A. Hably, S. Lesecq, J. Delamare, Bounded attitude control of rigid bodies: real-time experimentation to a quadrotor mini-helicopter. Control Eng. Pract. **19**(8), 790–797 (2011)

J.S. Jang, D. Liccardo, Small UAV automation using MEMS. IEEE Aerosp. Electron. Syst. Mag. **22**, 30–34 (2007)

T.S. Kim, K. Stol, V. Kecman, Control of 3 DOF quadrotor model, in *Robot Motion and Control 2007*, ed. by K. Kozlowski (Springer, London, 2007), pp. 29–38

I. Kroo, P. Kuns, Mesoscale flight and miniature rotorcraft development, in fixed and flapping wing aerodynamics for micro air vehicle applications, of progress in astronautics and aeronautics, **195**, pp. 503–517 (2001)

C. Lanczos, An iteration method for the solution of the eigenvalue problem linear differential and integral operators. J. Res. Natl. Bur. Stand. **45**, 255–282 (1950)

L. Meier, P. Tanskanen, F. Fraundorfer, M. Pollefeys, PIXHAWK: a system for autonomous flight using onboard computer vision, in *IEEE International Conference on Robotics and Automation*, Shanghai, 2011

D. Mellinger, M. Shomin, V. Kumar, Control of quadrotors for robust perching and landing, in *International Powered Lift Conference*, Philadelphia, Oct 2010

D. Mellinger, M. Nathan, V. Kumar, Trajectory generation and control for precise aggressive maneuvers with quadrotors. Int. J. Robot. Res. **31**(5), 664–674 (2012)

R.C. Michelson, Overview of micro air vehicle system design and integration issues, in *Encyclopedia of Aerospace Engineering*, ed. by R. Blockley, W. Shyy (Wiley, Chichester/Hoboken, 2010)

R. Naldi, L. Gentili, L. Marconi, A. Sala, Design and experimental validation of a nonlinear control law for a ducted-fan miniature aerial vehicle. Control engineering practice, Special issue on aerial robotics, **18**(7), pp. 747–760 (2010)

L. Petricca, P. Ohlckers, C. Grinde, Micro- and nano-air vehicles: state of the art. Int. J. Aerosp. Eng. **2011**, 1–17 (2011)

S.K. Phang, J.J. Ong, R. Yeo, B.M. Chen, T.H. Lee, Autonomous mini-UAV for indoor flight with embedded on-board vision processing as navigation system, in *IEEE Region 8 International Conference on Computational Technologies in Electrical and Electronics Engineering (SIBIRCON)*, Irkutsk Listvyanka, 2010

S.K. Phang, C. Cai, B.M. Chen, T.H. Lee, Design and mathematical modeling of a 4-standard-propeller (4SP) quadrotor, in *World Congress on Intelligent Control and Automation*, Beijing, 2012

P. Pounds, R. Mahony, J. Gresham, P. Corke, J. Roberts, Towards dynamically-favourable quadrotor aerial robots, in *Proceedings of the Australian Conference on Robotics and Automation*, Canberra, 2004

P. Pounds, R. Mahony, P. Corke, Modelling and control of a quad-rotor robot, in *Proceedings Australasian Conference on Robotics and Automation 2006*, Auckland, 2006

F. Wang, S.K. Phang, J. Cui, B.M. Chen, T.H. Lee, Search and rescue: a UAV aiding approach, in *Canadian Congress of Applied Mechanics*, Vancouver, June 2011

F. Wang, S.K. Phang, J. Cui, G. Cai, B.M. Chen, T.H. Lee, Nonlinear modeling of a miniature fixed-pitch coaxial UAV, in *American Control Conference*, Montreal, 27–29 June 2012

R.J. Wood, Design, fabrication and analysis of a 3DOF, 3 cm flapping-wing MAV, in *Proceedings of the 2007 IEEE/RSJ International Conference on Intelligent Robots and Systems*, San Diego, 29 Oct–2 Nov 2007

B. Yun, K. Peng, B.M. Chen, Enhancement of GPS signals for automatic control of a UAV helicopter system, in *Proceedings of IEEE International Conference on Control and Automation*, Guangzhou, 2007, pp. 1185–1189